Available online at www.sciencedirect.com
SCIENCE DIRECT®
ELSEVIER
Nuclear Instruments and Methods in Physics Research A 551 (2005) 145–151
NUCLEAR INSTRUMENTS & METHODS IN PHYSICS RESEARCH Section A
www.elsevier.com/locate/nima

Fast high-resolution characterization of powders using an imaging plate Guinier camera

Joseph Gal[a], Dmitry Mogilanski[a], Michael Nippus[b], Jacob Zabicky[a], Giora Kimmel[a,*]

[a]*Institutes for Applied Research, Ben-Gurion University of the Negev, Beer Sheva, Israel*
[b]*Huber Diffraktionstechnik GmbH & Co. KG, D-83253 Rimsting, Germany*

Available online 10 August 2005

Abstract

A new Huber Guinier camera G670 was installed on an Ultrax18-Rigaku X-ray rotating Cu anode source, with a monochromator (focal length $B = 360$ mm) providing pure $K\alpha_1$ radiation. The camera is used for powder diffraction applying transmission geometry. An imaging plate (IP) brings about position-sensitive detection measurement. In order to evaluate this new instrumental setup, quality data were collected for some classical reference materials such as silicon, quartz, some standards supplied by NIST USA and ceramic oxides synthesized in our laboratory. Each sample was measured at 4 kW for 1–2 min at 2θ from 0 to 100°. The results were compared with published references.

The following desirable features are noted for the instrumental combination studied: production of high quality X-ray data at a very fast rate, very accurate intensity measurements, sharp diffraction patterns due to small instrumental broadening and a pure monochromatic beam, and small position errors for 2θ from 4 to 80°. There is no evidence for extra line broadening by the IP camera detector setup. It was found that the relatively high instrumental background can be easily dealt with and does not pose difficulty in the analysis of the data. However, fluorescence cannot be filtered.

PACS: 01.03C; 06.70Ep; 07.85

Keywords: Imaging plate; X-ray diffractometry; Guinier camera; Standard reference materials; Materials characterization

1. Introduction

The Guinier camera is based on a monochromatic beam being transmitted through a powder sample and the diffracted beams being recorded on the focusing circle (Fig. 1). The oldest Guinier camera, also called focusing camera [1], used a

*Corresponding author.
E-mail addresses: jgal@bgu.ac.il (J. Gal), kimmel@bgu.ac.il (G. Kimmel).

0168-9002/$ - see front matter
doi:10.1016/j.nima.2005.07.048

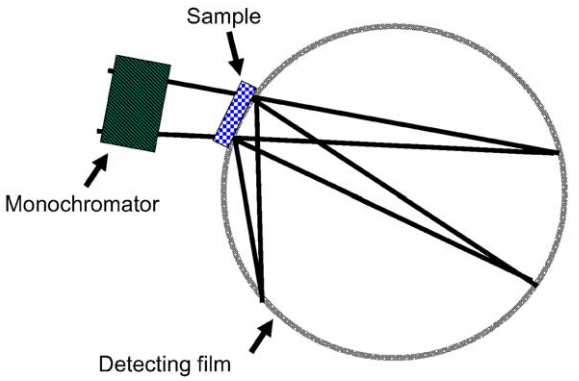

Fig 1. Schematics of the Guinier image plate camera (GIPC).

single crystal that served two purposes: separating the characteriztic beam from the white radiation and converging the diffracted beams into the focus circle. The diffraction pattern was recorded on an X-ray wet film, after a short exposure time of about 10 min. The diffraction lines were sharp with low background, except when fluorescence occurred. The main disadvantages of the film are poor sensitivity to the X-ray intensity and existence of a top limit to the radiation dose. On the other hand, there is no limit to the flux rate of the X-ray photons. Among the improvements introduced to this detection method system one counts the use of high quality crystals in the monochromator, resulting in a pure $K\alpha_1$ beam, and replacing the wet film by a counter to measure the scattered intensities obtained on scanning along the focusing circle in steps of about 0.01° on the 2θ scale [2]. The counting time for each step is 2–10 s, then, for a 2θ range of 90° and a counting time of 4 s/step the measuring time becomes 10 h. A position sensitive detector (PSD) was introduced later on to shorten the measuring time. However, PSDs based on gas ionization suffer from lack of accuracy for diffraction line positions. The efficiency of both counters decreases at high counting rates. The recent imaging plate (IP) detector seems to combine fast measurement with accurate diffraction line positioning. Unlike the wet film, the IP tolerates high exposure doses giving accurate intensity measurements. In addition, the diffraction line positioning on the IP is accurate and maintains linearity at very high counting rates, which is adequate for high-intensity X-ray sources, such as high-brilliance synchrotron sources [3–6].

When using a rotating anode source the IP is supposed to perform better than scintillation and gas detectors, which are inefficient at a high photon flux. The first choice for such an instrument was a Guinier IP camera (GIPC). By utilizing a double focal length of the Ge monochromator an increase of accuracy of the counting location at the expense of the intensity was achieved. This novel setup motivated us to evaluate the following properties of the setup: (a) accuracy of the intensity of the measured reflections for qualitative and quantitative phase analysis; (b) accuracy of line positioning for identification and quantitative elemental analysis of solid crystalline solutions; (c) instrumental broadening for efficient strain and size analysis; (d) signal to background ratio (SBR); and (e) analytical quality at short measuring times.

2. Experimental

2.1. Materials

The selected samples were powders with a variety of densities and unit cell dimensions. The following standard reference materials (SRM) of the National Institute for Standards and Technology (NIST), Maryland, USA were examined: for intensity the SRM 674a series: Al_2O_3 (corundum), CeO_2, Cr_2O_3, TiO_2 (rutile) and ZnO (wurtzite); for accuracy of line position, SRM 640 (Si) as light element, and W and Ag as heavy elements; and for instrumental line broadening as well as line position accuracy SRM 660: LaB_6. Oxide alloys $(Dy_xY_{1-x})_2O_3$, $(0 \leqslant x \leqslant 1)$, prepared in our laboratory were used for testing various aspects of X-ray diffraction analysis.

2.2. Instrumental

The new Huber Guinier camera G670 was installed on an Ultrax18-Rigaku X-ray rotating Cu anode source. The diffraction geometry is of Guinier type with the sample in transmission-asymmetric geometry, namely, angle of incidence

45° to sample normal. In these conditions, the sample moves asymptotically to the focal circle (see Fig. 1). The diameter of the focal circle of the monochromator is 360 mm. The diameter of the focal circle of the camera is 180 mm. The camera covers the 2θ range from 0 to 100°. The aluminum camera housing consists of two main parts: (a) the upper inner part of the camera cylinder holds the IP (a Fujifilm ST-Vn stripe), the erasing halogen lamp and the X-ray entrance window; and (b) the lower part contains an electro-mechanical device to actuate the readout unit. The beam of a red 635 nm diode laser is focused on the surface of the IP. The diffusely scattered blue photo-stimulated luminescence (PSL) light enters a photomultiplier tube (PMT) through a blue transmitting edge filter. The step motor clock triggers an A/D converter, i.e. each step of the driving motor generates a corresponding value of the PMT signal. A complete diffractogram for the 2θ range from 0 to 100° consists of 20,000 data points which corresponds to a step resolution of 0.005° 2θ. More details about the IP Guinier camera G670 are given in the website www.xhuber.com/er/diffractometer/guinier/670/670.htm.

2.3. Measurement procedure

The powders were adhered to a thin flat polyethylene (Mylar) foil attached to the sample holder with reciprocal movement parallel to the foil surface, in order to increase the illuminated area by the incident beam. The rotating anode was operated at 50 kV, 80 mA (4 kW). The exposure time usually was 2 min. The data recording was made by moving the readout system several times and accumulating the data. In most cases, three scanning runs of the readout system suffice to obtain a good quality diffractogram; however, additional runs can be made until no residual excitation remains on the IP. In this work five readout runs were carried out for all samples.

2.4. Analysis

The scan data were analyzed by conventional methods including fast peak search, line profile fitting for narrow 2θ ranges and whole pattern treatment (the Rietveld method [7]). For the line profile simulation, both for a single line and whole pattern treatment, a pseudo-Voigt function was used with asymmetry correction. The following characteriztics were found from the analysis: line positions, integrated intensities, line widths and relative intensity distribution. These data provide the structural information on unit cell parameters and atomic positions.

3. Results and discussion

3.1. Signal to background ratio (SBR)

Without X-ray excitation, it is known that the IP shows a nearly uniform background which contributes about 80 counts/pixel after the halogen lamp operation. This background is observed at all 2θ angles for each readout run. It is suggested to call this reading dark background, which should be considered as an instrumental bias. The dark background leads to the impression that the background is uniform. Actually, after subtracting the dark counting (about 400 counts for 5 readout runs) the background appearance is as expected for a Guinier camera.

Fig. 2 shows the diffractograms of α-quartz, in the 2θ range between 67° and 69°, obtained with the GIPC and a Bragg–Brentano diffractometer (BBD) with a gas proportional detector and a

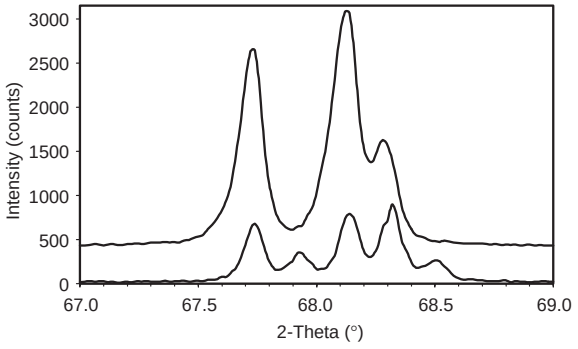

Fig. 2. Comparison between the X-ray diffractograms of α-quartz obtained with a Guinier G670 IP camera (upper trace) and a Bragg–Brentano diffractometer (lower trace). Intensities in counts of independent experiments.

graphite monochromator attached to the detector. The exposure time in GIPC was 120 s, and the source power was 4 kW. The BBD diffractograms were obtained with a 45 kV, 40 mA source and step scanning with 0.02° 2θ steps, measuring for 1 s/step. The BBD diffractogram shows doublet diffraction lines due to the unresolved $K\alpha_1/K\alpha_2$ beam from the source, whereas the GICP peaks are those diffracted from a pure $K\alpha_1$ beam. A significant difference is observed for the intensities, because the GICP counting rate is 6 times higher. Another difference is a higher background of about 435 counts for the GIPC which is absent for the BBD. After subtracting the dark background the background of the GIPC trace was 35 counts, which is comparable to the 20 counts of the BBD. The SBR of the strongest line in this range was 76 for the GIPC and 45 for the BBD.

The diffractograms of ZnO, WC and Cr_2O_3 appearing in Fig. 3 show different SBR. Moreover, none of these materials is considered to produce a severe background when working with Cu $K\alpha$ radiation and a conventional detector. In the present work samples are exposed to a monochromatic beam of Cu $K\alpha_1$ with a photon energy of 8.04778 keV, which can excite only Cr atoms. For ZnO, WC and Cr_2O_3, the background was 50, 10 and 100 counts above dark background at $2\theta = 30°$ and decreased to 5, 5 and 70 counts at $2\theta \geqslant 75°$, respectively. The $K\alpha_1$, $K\alpha_2$ and $K\beta$ radiation emitted from Cr, with photon energies of 5.41472, 5.405509, 5.94671 keV, respectively, cannot excite the L electrons of the Eu dopant in the IP film. On the other hand, the excitation of L electrons of Ba in the IP film by the Cr K emission lines is very effective. This may be the reason for the higher background shown in the Cr_2O_3 diffractogram. For the strongest lines in the 2θ range between 0° and 100°, after subtracting the dark background, the SBR was 100 for WC, 90 for ZnO and only 3 for Cr_2O_3.

3.2. Line characteriztics

The line shape, position and width are dictated by the material structure, grain size and microstrain on the one hand and instrumental aberrations on the other hand.

3.2.1. Line shape

The known pseudo-Voigt function used for line profile fitting worked well for the diffraction peaks obtained with the GIPC. For example, line profile fitting of the strongest Bragg reflection of tungsten (1 1 0), as shown in Fig. 4, points to excellent

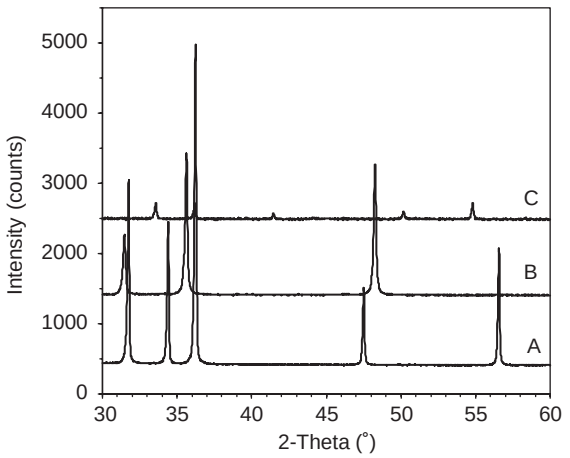

Fig. 3. Quality of the X-ray diffractograms of ZnO (A), WC (B, note counts shifted by 1000) and Cr_2O_3 (C, note counts shifted by 2000), obtained with a Guinier G670 IP camera under identical operation conditions (see experimental).

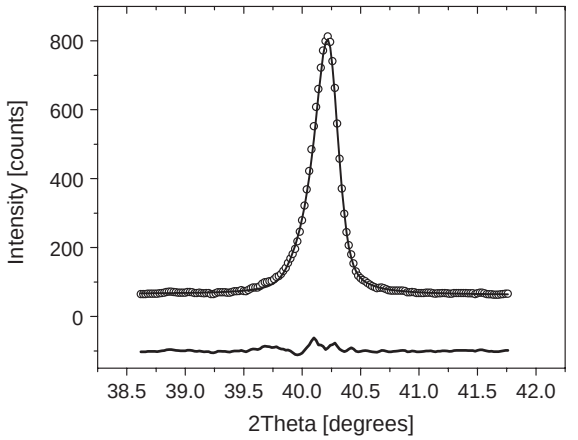

Fig. 4. Line profile of the 110 reflection of tungsten fitting. Legend: ○—experimental data, upper solid curve pseudo-Voigt including fit with asymmetric correction, lower solid curve is the difference (experimental fit).

agreement between the observed and the calculated counts.

3.2.2. Line position and width

LaB_6 powder (SRM 660) and Si (SRM 640) were used for evaluation of the line position accuracy of the instrument. After performing a line profile fitting it was found that at most of the 2θ range the angular deviation is less than 0.02° (see Tables 1 and 2). However, there is a systematic trend for positive error at the low angle range and negative error in the higher range (experimental−calculated angles). These errors are typical to sample displacement aberrations as described in the G670 website (see Section 2.2).

Accurate line positions are needed for determination of cell parameters. Table 3 gives measured and literature data [8–11] of cell parameters for SRM samples and commercial W, Ag and WC powders. The measured values in the present work are very close to the reported values from the literature. For example, the measured cell parameter of Si from GIPC data is 543.14 pm, whereas 543.12 pm is given by NIST.

A smooth function of the line widths versus the measured angles is indicative of reliable measurements. In Tables 1 and 2 it is shown that the line width increases for LaB_6 and Si uniformly with 2θ, as expected. It is readily seen in Table 1 that there is no significant difference between the FWHM values obtained with the GIPC when compared to those obtained with the BBD (both diffractometers are equipped with monochromators). Hence, there is no evidence that the IP contributes an additional instrumental broadening.

Another way to verify the accuracy of the GIPC is measuring the series of binary solid solutions. One expects to obtain a smooth dependence of the cell parameters on the composition. The selected rare earth cubic system, $(Dy_xY_{1-x})_2O_3$ $(0 \leqslant x \leqslant 1)$, shows a linear regression of the cell parameter a versus the atomic fraction x (Fig. 5), conforming to Vegard's rule for ideal solutions. Our results are in excellent agreement with published data [11]. The close linearity of these functions is indicative of the high quality of the measurements.

Table 1
Measured versus calculated 2θ values (°) of line positions and line widths of SRM 660a (LaB_6)

2θ-meas.	FWHM GIPC	FWHM BBD	2θ-cal.	*hkl*	2θ error
21.380	0.080	0.108	21.358	100	0.007
30.397	0.085	0.096	30.385	110	0.000
37.457	0.079	0.092	37.442	111	−0.002
43.518	0.080	0.087	43.507	200	−0.007
48.955	0.087	0.091	48.958	210	−0.018
53.991	0.083	0.095	53.989	211	−0.014
63.220	0.086	0.089	63.219	220	−0.014
67.544	0.089	0.102	67.548	300	−0.018
71.735	0.088	0.093	71.746	310	−0.021
75.839	0.099	0.101	75.844	311	−0.009
83.829	0.105	0.133	83.846	320	−0.016
87.761	0.117	0.114	87.792	321	−0.022

Measured values obtained by line profile fitting and calculated ones from the NIST certificate [9].

Table 2
Measured versus calculated 2θ values (°) of line positions and line widths of SRM 640, Si

2θ-meas.	FWHM	2θ-cal.	*hkl*	2θ error
28.446	0.072	28.441	111	0.014
47.291	0.081	47.300	220	0.010
56.116	0.083	56.120	311	0.005
69.108	0.090	69.126	400	−0.021
76.366	0.096	76.372	331	−0.002
87.984	0.127	88.025	422	−0.005
94.882	0.140	94.947	511	−0.032

Measured values obtained by line profile fitting and calculated ones from the NIST certificate [10].

Table 3
Measured versus published cell parameters (pm)

Material	*a*-meas.	*c*-meas.	*a*-reported	*c*-reported	Ref.
CeO_2	541.17	—	541.13	—	11
LaB_6	415.77	—	415.67	—	9
WC	290.63	283.87	290.63	283.79	8
ZnO	325.11	520.81	324.98	520.65	11
W	316.49	—	316.52	—	8
Ag	408.5	—	408.3	—	8
Si	543.14	—	543.12	—	10
Cr_2O_3	496.1	1360.6	495.9	1359.7	11
Al_2O_3	476.1	1299.6	475.9	1299.2	11

3.3. Integrated intensities

Integrated intensities are important for quantitative phase analysis and for structural analysis. A

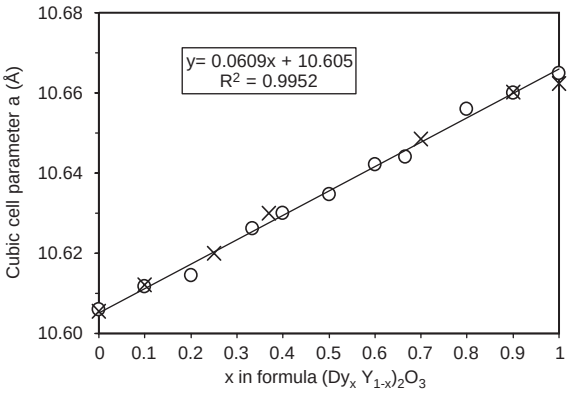

Fig. 5. Cell parameter a for the cubic structures (space group $Ia\bar{3}$) of $(Dy_xY_{1-x})_2O_3$ ($0 \leqslant x \leqslant 1$) as a function of the atomic fraction x in solid solutions, annealed in air for 12 h at 700 °C (○) and comparison with published data [12] (×). The linear regression is for ○.

Table 4
Rietveld analysis of WC

hkl	FWHM	2θ (°)	I-observed	I-calculated	I error (%)
001	0.196	31.465	21,451	21,295	0.73
100	0.193	35.617	50,378	49,179	2.38
101	0.193	48.262	49,108	49,166	−0.12
110	0.215	63.998	11,202	10,775	3.81
002	0.219	65.712	3456	3279	5.12
111	0.241	73.073	12,822	12,585	1.85
200	0.249	75.458	6171	6217	−0.75
102	0.255	77.055	11,688	11,680	0.07
201	0.286	84.04	10,358	10,265	0.90
112	0.374	98.664	7970	7966	0.05
					RB = 1.32%

correct measure of intensity is essential for accepting any detection method. The quality of the experimental intensity, when compared to the theoretical calculated integral intensities, is remarkable. The materials α-Al_2O_3, CeO_2, WC and ZnO were measured and analyzed by the Rietveld method. All the R_{BRAGG} values (Eq. 1) were below 0.04. Table 4 shows the intensity values of WC with $R_{BRAGG} = 0.016$, pointing to excellent quality.

$$R_{BRAGG} = \frac{\Sigma|I_{obs} - I_{cal}|}{\Sigma I_{obs}}. \quad (1)$$

3.4. General discussion

In contrast to conventional detectors (scintillation and gas proportional) which handle only the count intensity while the count position is treated by the goniometer control, the IP detector accounts for both count intensity and position, similarly to wet films and the PSD mentioned in Section 1. The present study shows that the errors in 2θ angles are in the range of the sample errors. The small instrumental broadening is typical to diffractometers with a monochromator. Hence the contribution of the detector to position aberration is not discernible.

It could be claimed that information stored in the IP detector is unstable and immediately starts to decay. In spite of the simultaneous exposure of the entire angle range, the readout obtained while the step scanning is in progress belongs to different phases of the decay. However, due to the fast multi-scan process it was found that the relative intensities over the whole angle range are extremely precise and accurate, and there is no evidence of intensity drift during the measurements. The precise position and intensity data afford excellent results in whole pattern treatment. The detector was found to be very stable as demonstrated by 12 solid-solution samples of composition $(Dy_xY_{1-x})_2O_3$ ($0 \leqslant x \leqslant 1$), the cell parameters of which show a linear dependence on the atomic fraction x in the solid solutions (Fig. 5).

The SBR of the IP detector is different from that of conventional detectors. The diffractogram of chromium oxide is only one example of very poor SBR due to unexpected excitation of the detector by the fluorescent Cr Kα radiation. With a conventional system (BBD with gas or scintillation detector and Cu Kα source) the Cr_2O_3 sample shows an SBR of 72 as compared to 3 with GIPC. However, materials which are far enough from the absorption edge of the IP active components show SBR similar to that obtained with the conventional systems.

It should also be mentioned that the measuring time for the quartz sample (Fig. 2) with the GIPC was about 100-fold that of the conventional system, while the source power was only 2.5-fold stronger. Nevertheless, the neat intensities after subtracting the dark background were only about

10-fold for GIPC. Several reasons may be adduced for this dimmed signal enhancement: (a) the primary beam monochromator decreases the beam intensity; (b) the distance of the sample from the source is longer than usual; (c) the IP detector is apparently less efficient than the gas proportional detector.

4. Summary and conclusions

The combination of a high power source (rotating anode) and a digital camera (IP) was tested. A variety of powders were selected to evaluate the performance of this instrument, including SRM and other powders of different densities and composition. Data were collected in a short time (2 min) while operating the source at a power of 4 kW. It was found that the IP detector is very accurate and stable for line position and intensity, which are collected simultaneously. The intensities show very accurate and very low R_{BRAGG} factors, which were calculated for compounds of known structures. The only aberrations found in peak positions were caused by the sample thickness, introducing displacement errors.

For samples containing certain elements (e.g., Cr) the SBR may be very low due to absence of filtering of fluorescence and further non-elastic scattering from the sample. Otherwise, the SBR is about 100 for the strongest line, which is similar to the behavior of conventional systems. Nevertheless, the SBR is at least 10 times better than a conventional BBR system. The IP detector was found to be a good choice for a Guinier camera equipped with a rotating anode source. The combination of accurate intensity and position data makes the GIPC an excellent detector for quantitative and structural analysis.

Acknowledgements

The authors wish to thank the Planning & Budgeting Committee of the Council for Higher Education of Israel (VATAT) for financial support.

References

[1] J.B. Cohen, Diffraction Methods in Materials Science, The Macmillan Company, New York, 1966.
[2] L.S. Zevin, G. Kimmel, Quantitative X-ray Diffractometry, Spriger, New York, 1995.
[3] Y. Amemiya, Imaging plates for use with synchrotron radiation, J. Synchrotron. Radiat. 2 (1995) 13.
[4] C. Meneghini, G. Atrioli, A. Balerna, A.F. Gualtieri, P. Norby, S. Mobilio, Multipurpose imaging-plate camera for in-situ powder XRD at the GILDA beamline, J. Synchrotron. Radiat. 8 (2001) 1162.
[5] O. Stachs, T. Gerber, V. Petkov, An image plate chamber for X-ray diffraction experiments in Debye-Scherrer geometry, Rev. Sci. Instrum. 71 (2000) 4007.
[6] K. Ståhl, J. The Huber G670 imaging-plate Guinier camera tested on beamline I711 at the MAX II synchrotron, J. Appl. Crystallogr. 33 (2000) 394.
[7] R.A. Young, DBWS-9411-an upgrade of the DBWS programs for Rietveld Refinement with PC and mainframe computers, J. Appl. Crystallogr. 28 (1995) 366.
[8] P. Villars, L.D. Calvert, Pearson Handbook of Crystallographic Data for Intermetallic Phases, ASM, USA, 1986.
[9] NIST, USA, certificate SRM 660a
[10] NIST, USA, certificate SRM 640c
[11] NIST, USA, certificate SRM 674a
[12] B. Antic, P. Önnerud, D. Rodic, R. Tellgren, The structures characteristics of dilute magnetic semiconductor $Y_{2-x}Dy_xO_3$, Powder Diffract. 8 (1993) 216.